Chapter 6

Localized states influence spin transport in epitaxial graphene

This chapter appeared in Physical Review Letters **110**, 235428 (2014).
Authors: T. Maassen, J. J. van den Berg, E. H. Huisman, H. Dijkstra, F. Fromm, T. Seyller, and B. J. van Wees.

Abstract

We developed a spin transport model for a diffusive channel with coupled localized states that result in an effective increase of spin precession frequencies and a reduction of spin relaxation times in the system. We apply this model to Hanle spin precession measurements obtained on monolayer epitaxial graphene on SiC(0001) (MLEG). Combined with newly performed measurements on quasi-free-standing monolayer epitaxial graphene on SiC(0001) our analysis shows that the different values for the diffusion coefficient measured in charge and spin transport measurements in MLEG and the high values for the spin relaxation time can be explained by the influence of localized states arising from the buffer layer at the interface between the graphene and the SiC surface.

6.1 Introduction

The spin dynamics in the diffusive transport regime are in general described by the Bloch equation for the spin chemical potential $\vec{\mu}_S$ that describes the three dimensional spin accumulation:[1]

$$\frac{d\vec{\mu}_S}{dt} = D\nabla^2\vec{\mu}_S - \frac{\vec{\mu}_S}{\tau_S} + \vec{\omega}_L \times \vec{\mu}_S \tag{6.1}$$

with the diffusion coefficient D, the spin relaxation time τ_S and the Larmor frequency $\vec{\omega}_L = g\mu_B/\hbar\ \vec{B}$, that describes the spin precession in a perpendicular magnetic field $\vec{B}$ with the gyromagnetic factor g (g-factor, $g = 2$ for free electrons) and the Bohr magneton μ_B. Experimentally, spin transport is commonly examined by Hanle spin precession measurements (Fig. 6.1a) that are fitted with the solutions of the time independent Bloch equation (6.1) with $d\mu_S/dt = 0$. Those fits result in D, τ_S and the spin relaxation length $\lambda_S = \sqrt{D\tau_S}$. However, the fits are invariant under the transformation $D \to c\tilde{D}$, $\tau_S \to \tilde{\tau_S}/c$, $g \to c\tilde{g}$ leaving the scaling factor c undefined. To unambiguously define the parameters, D can be independently determined using

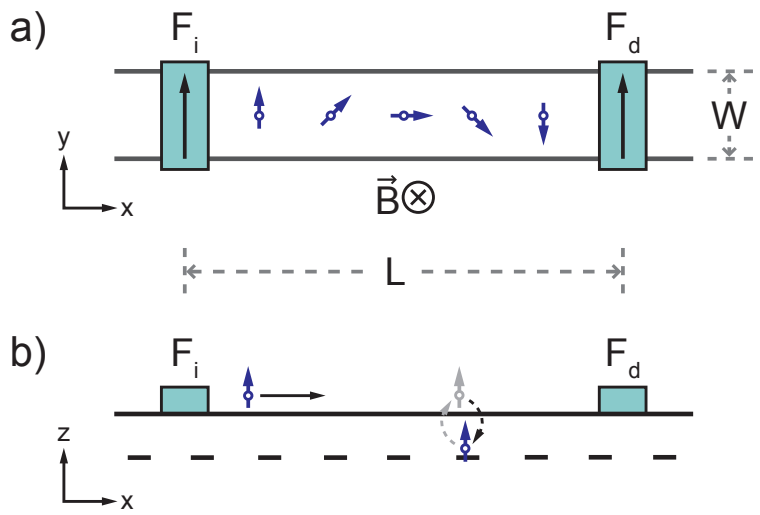

Figure 6.1: (Color online) (a) Sketch of the Hanle precession geometry with a diffusive channel of width W connected to the ferromagnetic spin injector (F_i) and detector (F_d) on distance L. The out-of-plane magnetic field $\vec{B}$ causes the in-plane injected spins to precess while diffusing through the channel. (b) Extension of the Hanle precession geometry with localized states that are coupled to the channel. The spins can hop into these states and back into the channel while the states are not coupled with each other.

the diffusion coefficient from charge transport measurements D_C and the Einstein relation $D_C = (R_{sq} e^2 \nu(E_F))^{-1}$.[a] Here R_{sq} is the square resistance, e the electron charge and $\nu(E_F)$ the density of states (DOS) of the diffusive channel at the Fermi energy.
Spin transport in graphene has been extensively studied in recent years.[2–15] Due to weak spin-orbit coupling, $g = 2$ is commonly assumed to fit Hanle precession data (and define c).[2–14] This was justified for exfoliated single layer graphene (eSLG) as it was shown that $D \approx D_C$.[4] On the contrary, recent results on monolayer epitaxial graphene on SiC(0001) (MLEG)[16, 17] show $D \ll D_C$ along with very high values for τ_S.[10b]
In this letter we introduce a model that can explain an apparent difference between D and D_C by the increase of the effective g-factor caused by localized states coupled to the spin transport channel. Furthermore, we discuss how this model reinterprets the results on MLEG from Ref.[10] and finally, we compare the results on MLEG to new Hanle precession measurements on quasi-free-standing MLEG on SiC(0001) (QFMLG).[18] In this material the graphene-like, electrical neutral buffer layer, that is in

[a] Note that for a diffusive channel generally impurity scattering dominates and $D = D_C$ holds, while a difference can arise due to strong electron-electron interactions e.g. in a two-dimensional electron gas as discussed by Weber et al., Nature (London) **437**, 1330 (2005)

[b] The results for MLEG from Ref. 11 using 4H-SiC have been reproduced in our lab for 6H-SiC.

conventional MLEG located between graphene and the SiC substrate, is absent.[19, 20] The presented analysis points to the buffer layer as the origin of the localized states.

6.2 Spin transport model

To examine the spin transport properties of graphene, usually the non-local measurement geometry is used, consisting of a two dimensional channel with ferromagnetic electrodes that inject and detect electron spins in the graphene plane [c2] (Fig. 6.1a). We extend this description with localized states in close proximity to the channel (Fig. 6.1b). We assume the states are electrically coupled to the channel and not coupled with each other.
The spin accumulation in the localized states is represented by $\vec{\mu}_S^*$ and its dynamics can be described by a Bloch equation similar to (6.1) that does not include a diffusive term but a term for the coupling to the channel.

$$\frac{d\vec{\mu}_S^*}{dt} = -\frac{\vec{\mu}_S^*}{\tau_S^*} + \vec{\omega}_L^* \times \vec{\mu}_S^* - \Gamma(\vec{\mu}_S^* - \vec{\mu}_S) \tag{6.2}$$

The Lamor frequency in the localized states $\vec{\omega}_L^* = \omega_L^* \hat{z} \equiv \alpha\omega_L \hat{z}$ can be different from $\vec{\omega}_L$ due to a possibly different g-factor $g^* \equiv \alpha g$. $\tau_S^* \equiv \beta\tau_S$ is the spin relaxation time of the localized states and the term $-\Gamma(\vec{\mu}_S^* - \vec{\mu}_S)$ describes the flow of spins from the localized states to the channel and vice versa with the coupling rate $\Gamma = (Re^2\nu_{LS})^{-1}$, where $1/R$ is the conductance per unit area between the localized states and the channel and ν_{LS} the density of localized states.[d,e]
To describe the spin dynamics in the channel we also have to add on the right side of the Bloch equation (6.1) a coupling term

$$\frac{d\vec{\mu}_S}{dt} = D\nabla^2\vec{\mu}_S - \frac{\vec{\mu}_S}{\tau_S} + \vec{\omega}_L \times \vec{\mu}_S - \eta\Gamma(\vec{\mu}_S - \vec{\mu}_S^*). \tag{6.3}$$

Here we introduce the factor $\eta \equiv \nu_{LS}/\nu$ that accounts for the different DOS in the channel ν compared to the localized states.
The two coupled equations (6.2) and (6.3) can be reduced to *one* effective Bloch equation. For this purpose we consider the system to be in a stationary state with $\frac{d\vec{\mu}_S^*}{dt} = 0$,

[c] The spins are injected in the plane for small magnetic fields that do not tilt the magnetization of the electrodes out-of-plane.

[d] We assume that the spin orientation is conserved in the coupling process.

[e] See Supplemental Material for the discussion of the coupling rate between the localized states and the graphene channel.

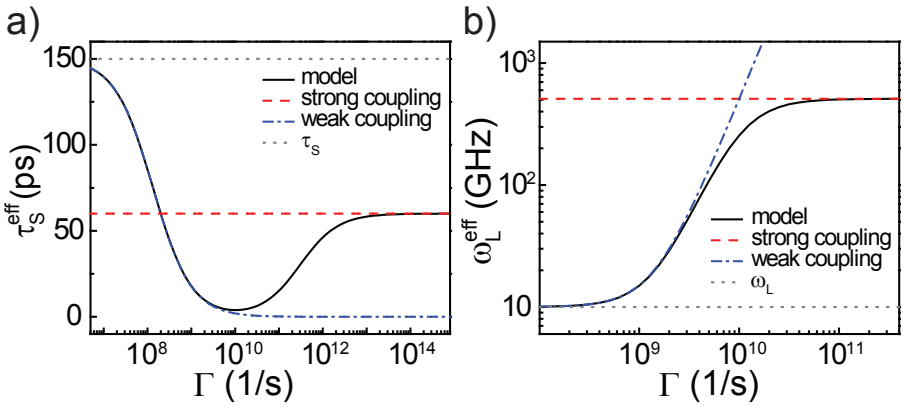

Figure 6.2: (Color online) The effective spin relaxation time τ_S^{eff} (a) and Lamor precession frequency ω_L^{eff} (b) as a function of the coupling rate Γ (black solid curves). The asymptotic values in the limit of strong (red, dashed curves) and weak coupling (blue, dash dotted curves). In the graphs we keep $\tau_S = 150$ ps (gray dotted curve in panel (a)), $\tau_S^* = 5$ ns, $\omega_L = 10$ GHz (for a magnetic field of $B \approx 50$ mT, gray dotted curve in panel (b)) and $\eta = 50$ constant.

rewriting equation (6.2) to $\vec{\mu}_S^* = \underline{a} \cdot \vec{\mu}_S$ with

$$\underline{a} = \frac{\tau_S^* \Gamma}{(\tau_S^* \Gamma + 1)^2 + (\tau_S^* \omega_L^*)^2} \times \begin{pmatrix} \tau_S^* \Gamma + 1 & -\tau_S^* \omega_L^* & 0 \\ \tau_S^* \omega_L^* & \tau_S^* \Gamma + 1 & 0 \\ 0 & 0 & \tau_S^* \Gamma + 1 + \frac{(\tau_S^* \omega_L^*)^2}{\tau_S^* \Gamma + 1} \end{pmatrix}. \tag{6.4}$$

As the spin accumulation is purely perpendicular to the magnetic field in the Hanle geometry ($\vec{\omega}_L \parallel \vec{\omega}_L^* \parallel \vec{B} \parallel \hat{z} \perp \vec{\mu}_S$) we get the effective Bloch equation

$$0 = D\nabla^2 \vec{\mu}_S - \frac{\vec{\mu}_S}{\tau_S^{\text{eff}}} + \vec{\omega}_L^{\text{eff}} \times \vec{\mu}_S. \tag{6.5}$$

Here we introduce the effective spin relaxation time τ_S^{eff} and the effective precession frequency of the system $\vec{\omega}_L^{\text{eff}} = \omega_L^{\text{eff}} \hat{z}$ defined by

$$\frac{1}{\tau_S^{\text{eff}}} = \frac{1}{\tau_S} + \eta\Gamma \frac{1 + \tau_S^* \Gamma + (\tau_S^* \omega_L^*)^2}{(1 + \tau_S^* \Gamma)^2 + (\tau_S^* \omega_L^*)^2} \tag{6.6}$$

$$\text{and} \quad \omega_L^{\text{eff}} = \omega_L + \eta\Gamma^2 \frac{(\tau_S^*)^2 \omega_L^*}{(1 + \tau_S^* \Gamma)^2 + (\tau_S^* \omega_L^*)^2}. \tag{6.7}$$

The expressions for τ_S^{eff} and ω_L^{eff} are plotted in Fig. 6.2 as a function of the coupling rate Γ (black solid curves). Note that independent from the value of Γ (or the value of η, τ_S^* or α) the model shows a decrease of τ_S^{eff} and an increased ω_L^{eff}.

For weak coupling, $\Gamma \ll 1/\tau_S^*$ (Fig. 6.2, blue dash dotted curves), we have long dwell times for the spins in the localized states and therefore $\tau_{dwell} \gg \tau_S^*$. As a consequence all the spins that hop into the localized states will relax before returning into the channel and are therefore "lost" for the spin transport. We get $1/\tau_S^{eff} \approx 1/\tau_S + \eta\Gamma$, while $\omega_L^{eff} = \omega_L + \mathcal{O}((\tau_S^*\Gamma)^2)$ stays approximately constant.
For strong coupling, $\Gamma \gg 1/\tau_S^*$ (Fig. 6.2, red dashed curves), we have to distinguish two cases. For $\omega_L^* \gg \Gamma$, we get the same result for τ_S^{eff} and ω_L^{eff} as for weak coupling. The strong precession in the localized states dephases all spins that hop into these states and they are lost.
The most interesting is the case of strong coupling, $\Gamma \gg 1/\tau_S^*$, and low precession frequencies, $\omega_L^* \ll \Gamma$, corresponding to the measurements in MLEG (see below). We get: $1/\tau_S^{eff} = 1/\tau_S + \eta/\tau_S^*$ and $\omega_L^{eff} = \omega_L + \eta\omega_L^*$. Both values are in this limit independent from the coupling rate Γ (Fig. 6.2). Note that we get an increased ω_L^{eff} also for $\omega_L = \omega_L^*$ ($g = g^*$). This is due to the fact that that spins dwelling in the localized states account for additional precession and relaxation, but they do not contribute to diffusion.

6.3 Comparison of the model with spin transport data

How does this model relate to the results on spin transport in MLEG on SiC(0001) reported in Ref.[10]? Here an increased τ_S and a strongly reduced diffusion coefficient ($D \ll D_C$) were observed. As mentioned before, $g = 2$ was assumed in Ref.[10] as there was no reason to assume a change of the g-factor for the graphene channel itself e.g. a changed spin-orbit coupling. But in graphene combined with localized states, with $\omega_L^{eff} \equiv \xi\omega_L > \omega_L$ and hence $g^{eff} \equiv \xi g$, this assumption presents itself wrong. The values that are obtained by fitting assuming $g = 2$ are described by a modified Bloch equation that we receive by dividing (6.5) by the scaling factor ξ:

$$0 = D^{mod}\nabla^2\vec{\mu}_S - \frac{\vec{\mu}_S}{\tau_S^{mod}} + \vec{\omega_L} \times \vec{\mu}_S \tag{6.8}$$

with $D^{mod} = D/\xi$ and $\tau_S^{mod} = \xi\tau_S^{eff}$. The effective spin relaxation time of the system including the localized states can be obtained by either assuming $D = D_C$ for the fit or assuming $g = 2$ and correcting the spin relaxation time with $\tau_S^{eff} = \tau_S^{mod}/\xi$. The enhanced τ_S value in Ref.[10] is therefore not an intrinsic property of MLEG on SiC(0001) but is based on assuming a Bloch equation to fit the data which does not take the localized states into account.
Note that the measured spin relaxation length does not change when assuming a different g-factor as $\lambda_S^{mod} = (D^{mod}\tau_S^{mod})^{1/2} = (D\tau_S^{eff})^{1/2} = \lambda_S^{eff} < \lambda_S$.
The narrow room temperature (RT) Hanle precession measurements on MLEG on SiC(0001)[10] in the center of Fig. 6.3 illustrate the effect of a modified g-factor. The fit

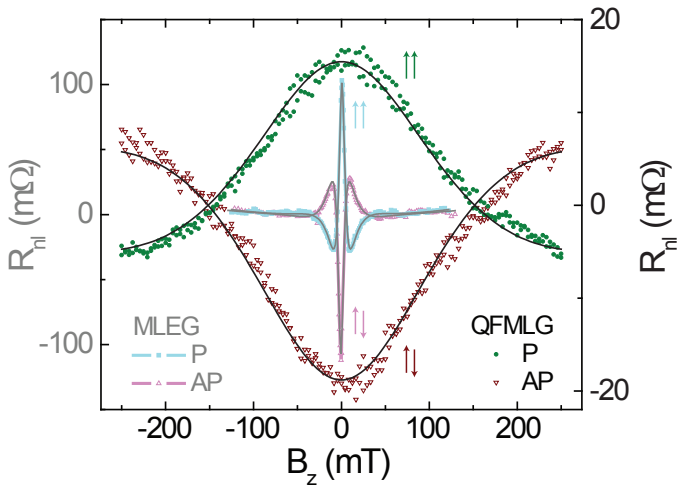

Figure 6.3: (Color online) RT Hanle precession measurements with aligned (↑↑) and antialigned (↑↓) inner electrodes. The narrow curves in the middle (light colors, scale on the left axis) show a measurement on MLEG with $L = 1.2$ ¯m and $W = 0.7$ ¯m from Ref.[10] The broader measurements enclosing the MLEG measurements (dark colors, scale on the right axis) were performed on QFMLG with $L = 1.5$ ¯m and $W = 1$ ¯m. The Hanle fits are plotted in gray. For both sets of measurements a constant background resistance was subtracted.

to this data (assuming $g = 2$) gives $\tau_S^{mod} = 1.3$ ns and $D^{mod} = 2.4$ cm^2/s, resulting in $\lambda_S^{eff} = 0.56$ ¯m. Compared to values obtained on eSLG[4] τ_S^{mod} is increased and D^{mod} is strongly reduced in contrast to the value of $D_C \approx 190$ cm^2/s obtained in charge transport measurements on the same sample and compared to $D \sim 200$ cm^2/s typically measured on eSLG.[4f] At RT this discrepancy between D^{mod} and D_C is resolved using a scaling factor of $\xi = D_C/D^{mod} \approx 190/2.4 \approx 80$, which yields a spin relaxation time of $\tau_S^{eff} \approx 1.3$ ns$/80 \approx 16$ ps and an effective g-factor of $g^{eff} \approx 80g$. Note that these values for τ_S^{eff} and g^{eff} are not describing only the graphene layer but the overall system, including the localized states.

To find out where the predicted localized states originate from, we prepared and measured spin transport samples on quasi-free-standing MLEG (QFMLG) as in Ref.[10] QFMLG is obtained by only growing the electrical neutral buffer layer and no graphene on SiC(0001) and then intercalating the sample by hydrogen as described in Refs.[19] and.[20] Then we are left with a single graphene layer directly on the passivated SiC(0001) surface.

Fig. 6.3 shows Hanle precession curves measured on a QFMLG strip at RT next to the measurements on MLEG from Ref.[10] The non-local resistance[2, 10] changes slower

[f]With comparable D_C in both systems, the transport is still dominated by impurity scattering.

with $\vec{B}$,[g] comparable to measurements performed on eSLG.[4] The fit (assuming $g = 2$) gives $\tau_S = 33.6 \pm 0.9$ ps and $D = 75 \pm 2$ cm^2/s and therefore $\lambda_S = 0.50 \pm 0.01$ ¯m.
These values are similar to low quality eSLG samples as τ_S is reduced by about a factor 4 and D by a factor of approximately 3 compared to typical eSLG values.[4] Compared to MLEG we see an increase of D by a factor of ~ 30 and a decrease of τ_S by about 40 times. In contrast to the MLEG data we see in charge transport measurements on similar QFMLG samples a diffusion coefficient of $D_C \approx 45$ cm^2/s $\sim D$.[h] To obtain D_C we use $R_{sq} \approx 3.5$ kΩand a hole charge carrier density of $p \approx 6 \times 10^{12}$ cm^{-2} from Hall measurements consistent with results from Ref.[20]
Comparing the results on the two graphene types on SiC(0001) it is interesting to see the striking difference of the spin relaxation times and diffusion coefficients obtained in spin transport measurements but even more important that $D_C \approx D$ in QFMLG, as expected for graphene.[4] Hence, there is no effect of the localized states. Accordingly, they have their origin in the interface between the graphene layer and the SiC substrate as this is the only structural property that is altered between conventional MLEG and QFMLG. Hence, the states could be in the dangling bonds or in the buffer layer. The strong difference of D vs D_C (and change in ω_L) reported in Ref.[10] points to a strong coupling of the localized states to the channel (see eq. 6.7) and Fig. 6.2b). The coupling is strongest if the localized states are located in the buffer layer as this one is closest to the channel. If we assume comparable coupling of these states to the channel and between adjacent layers in graphite and considering $\eta \sim 50$ (see below), we get $\Gamma \sim 2 \times 10^{13}$ s^{-1}, justifying the strong coupling limit (see Fig. 6.2).
Now we can evaluate the model and characterize the localized states by comparing the fitting results on MLEG on SiC(0001)[10] with data obtained on other types of monolayer graphene. To compensate for different D_C-values obtained in charge transport measurements on QFMLG and conventional MLEG, we use data on eSLG[4] to compare with results on conventional MLEG.[10] In the limit of strong coupling we get based on (6.8): $\xi = 1 + \alpha\eta$. Using the typical eSLG values, $\tau_S = 150$ ps and $D_C = D = 200$ cm^2/s, as the graphene values in the absence of localized states and the MLEG values as D^{mod} and τ_S^{mod} we get $\xi \approx \eta \approx 80$ at RT, assuming $g^* = g$ ($\alpha = 1$). Together with $\tau_S^{mod}/\tau_S \approx 9$ we obtain $\tau_S^*/\tau_S = \beta \approx 10$. Hence, at RT spins relax in the localized states with $\tau_S^* \approx 1.5$ ns about 10 times slower than in the graphene channel. This enhanced value is very reasonable for a confined state in a material with low spin-orbit coupling.
The presence of localized states can also explain the temperature dependence of spin transport in Ref.[10] in contrast to negligible change for eSLG.[2] By assuming the same values as before for D and τ_S in the absence of localized states, we get with the

[g] In the two measurements L is slightly different (1.2 ¯m vs. 1.5 ¯m) which has a minor influences on the width of the curve (FWHM $\sim 1/L$). The difference in the amplitude is not related to λ_S, which is comparable, but to a different contact polarization. There is no evidence that the minor change in W (0.7 ¯m vs. 1 ¯m) has a significant influence on the measurements.

[h] With comparable D_C in both systems, the transport is still dominated by impurity scattering.

data for MLEG at 4 K $\eta \approx 45$ and $\beta \approx 22$ ($\tau_S^* \approx 3.3$ ns). These results imply less accessible localized states with longer spin relaxation times at low temperature. By assuming a Boltzmann distribution we get from the change in η an activation energy of $E_a \approx 15$ meV.
Within our analysis, η describes the ratio of the DOS in the localized states and the channel. With η up to 80 we need a high density of localized states in our system. In MLEG with an electron charge carrier density of $n \approx 3 \times 10^{12}$ cm^{-2}[10] we have a DOS of $\nu \approx 3 \times 10^{13}$ eV^{-1}cm^{-2}. With a density of carbon atoms in the graphene-like buffer layer of 3.8×10^{15} cm^{-2} and assuming that every carbon atom contributes one localized state, we get $\eta = 80$ if these states are e.g. uniformly distributed over an energy range of ~ 1 eV. Those localized states can be the origin of the strong doping observed in MLEG on SiC(0001).[21]
The observed increase of g in MLEG could in principle also be related to magnetic moments induced by the buffer layer or dangling bonds on the surface of SiC(0001) as described for hydrogenated graphene in Ref.[13] We argue that this does not apply here since: i) The effect in MLEG is stronger at RT than at 4 K in contrast to only low temperature effects in hydrogenated graphene. ii) We do not see any effects resulting from randomized magnetic moments at low magnetic fields like the "dip" in the spin-valve measurements in Ref.[13] iii) The increase of g in MLEG is much bigger than in hydrogenated graphene.

6.4 Conclusions

To summarize, we developed a spin transport model for a diffusive channel with coupled localized states that results in an increased effective g-factor and a reduced spin relaxation time for the transported spins. This model can be applied to any nanoscale systems, where spin transport occurs via extended states which are coupled to localized states. We use it to reinterpret the data from Ref.[10] where an enhanced spin relaxation time and a reduced spin diffusion coefficient were observed. By comparing the data from Ref.[10] to new measurements on QFMLG and typical values on eSLG we identified the buffer layer as possible source for the localized states and the measurements can be related to a g-factor of $g^{\text{eff}} = (45 - 80)g$. Finally we use the model to characterize the spin properties of the localized states in the buffer layer of MLEG on SiC(0001).

References

[1] J. Fabian, A. Matos-Abiague, C. Ertler, *et al.* 'Semiconductor Spintronics'. *Acta Phys. Slov.* **57**, 565 (2007).

[2] N. Tombros, C. Józsa, M. Popinciuc, *et al.* 'Electronic Spin Transport and Spin Precession in Single Graphene Layers at Room Temperature'. *Nature (London)* **448**, 571 (2007).

[3] M. Popinciuc, C. Józsa, P. J. Zomer, *et al.* 'Electronic Spin Transport in Graphene Field-Effect Transistors'. *Phys. Rev. B* **80**, 214427 (2009).

[4] C. Józsa, T. Maassen, M. Popinciuc, *et al.* 'Linear Scaling Between Momentum and Spin Scattering in Graphene'. *Phys. Rev. B* **80**, 241403 (2009).

[5] W. Han, K. Pi, K. M. McCreary, *et al.* 'Tunneling Spin Injection into Single Layer Graphene'. *Phys. Rev. Lett.* **105**, 167202 (2010).

[6] A. Avsar, T.-Y. Yang, S. Bae, *et al.* 'Toward Wafer Scale Fabrication of Graphene Based Spin Valve Devices'. *Nano Lett.* **11**, 2363 (2011).

[7] W. Han and R. K. Kawakami. 'Spin Relaxation in Single-Layer and Bilayer Graphene'. *Phys. Rev. Lett.* **107**, 047207 (2011).

[8] T.-Y. Yang, J. Balakrishnan, F. Volmer, *et al.* 'Observation of Long Spin-Relaxation Times in Bilayer Graphene at Room Temperature'. *Phys. Rev. Lett.* **107**, 047206 (2011).

[9] S. Jo, D.-K. Ki, D. Jeong, *et al.* 'Spin Relaxation Properties in Graphene Due to Its Linear Dispersion'. *Phys. Rev. B* **84**, 075453 (2011).

[10] T. Maassen, J. J. van den Berg, N. IJbema, *et al.* 'Long Spin Relaxation Times in Wafer Scale Epitaxial Graphene on SiC(0001)'. *Nano Lett.* **12**, 1498 (2012).

[11] M. H. D. Guimares, A. Veligura, P. J. Zomer, *et al.* 'Spin Transport in High-Quality Suspended Graphene Devices'. *Nano Lett.* **12**, 3512 (2012).

[12] J. Abel, A. Matsubayashi, T. Murray, *et al.* 'Fabrication of an Electrical Spin Transport Device Utilizing a Diazonium Salt/Hafnium Oxide Interface Layer on Epitaxial Graphene Grown on 6 H-SiC(0001)'. *J. Vac. Sci. Technol. B* **30**, 04E109 (2012).

[13] K. M. McCreary, A. G. Swartz, W. Han, *et al.* 'Magnetic Moment Formation in Graphene Detected by Scattering of Pure Spin Currents'. *arXiv:1206.2628v1* (2012).

[14] M. Wojtaszek, I. J. Vera-Marun, T. Maassen, *et al.* ArXiv:1209.2365v1.

[15] B. Dlubak, M.-B. Martin, C. Deranlot, *et al.* 'Highly Efficient Spin Transport in Epitaxial Graphene on SiC'. *Nature Phys.* **8**, 557 (2012).

[16] C. Virojanadara, M. Syväjarvi, R. Yakimova, *et al.* 'Homogeneous Large-Area Graphene Layer Growth on 6H-SiC(0001)'. *Phys. Rev. B* **78**, 245403 (2008).

[17] K. V. Emtsev, A. Bostwick, K. Horn, *et al.* 'Towards Wafer-Size Graphene Layers by Atmospheric Pressure Graphitization of Silicon Carbide'. *Nature Mater.* **8**, 203 (2009).

[18] J. J. van den Berg. Et al. in preparation.

[19] C. Riedl, C. Coletti, T. Iwasaki, *et al.* 'Quasi-Free-Standing Epitaxial Graphene on SiC Obtained by Hydrogen Intercalation'. *Phys. Rev. Lett.* **103**, 246804 (2009).

[20] F. Speck, J. Jobst, F. Fromm, *et al.* 'The Quasi-Free-Standing Nature of Graphene on H-Saturated SiC(0001)'. *Appl. Phys. Lett.* **99**, 122106 (2011).

[21] S. Kopylov, A. Tzalenchuk, S. Kubatkin, *et al.* 'Charge Transfer Between Epitaxial Graphene and Silicon Carbide'. *Appl. Phys. Lett.* **97**, 112109 (2010).

[22] K. Matsubara, K. Sugihara, and T. Tsuzuku. 'Electrical Resistance in the c Direction of Graphite'. *Phys. Rev. B* **41**, 969 (1990).

Supplementary information

Coupling rate between the localized states and the graphene channel

To estimate the coupling rate Γ between the localized states and the graphene channel, we can set up a simplified model based on the coupling between adjacent graphene layers in graphite, as these layers have the same or similar physical distance as the buffer layer to the graphene layer.
In graphite, the conductance in z-direction perpendicular to the layers is per layer $\sigma_{\mathrm{IL}} = \sigma_{\mathrm{gr}}/(\zeta d)$ where σ_{gr} is the in-plane conductivity of a graphene layer, d the distance between two layers (or between the graphene layer and the localized states) and $\zeta \approx 100$ the ratio between the conductivity within the layers and perpendicular to them.[22]
We can now calculate for a current I_{IL} in z-direction:

$$I_{\mathrm{IL}} = \frac{V\sigma_{\mathrm{IL}}A}{d} = \frac{dQ}{dt} = e\frac{dN}{dt} = e\nu_{\mathrm{LS}}\frac{d\mu}{dt}A \tag{6.9}$$

Here $V = \mu/e$ is the voltage between the localized states and the channel, proportional to the difference in the chemical potential, A the area through which the current flows, Q is the total charge that flows, N the number of charge carriers, d is the distance to and ν_{LS} the density of states (DOS) of the localized states, and e the electron charge.
Using the Einstein relation with ν the DOS and D the diffusion coefficient of the graphene channel we get:

$$V\frac{\nu}{\nu_{\mathrm{LS}}}\frac{D}{d^2}\frac{1}{\zeta} = \frac{dV}{dt} \tag{6.10}$$

This equation includes the ratio of the DOS of the localized states and the graphene channel $\eta = \nu_{\mathrm{LS}}/\nu$ that was discussed in the main text of this letter.
With the coupling rate $\Gamma \sim \frac{1}{V}\frac{dV}{dt}$ we receive :

$$\Gamma = \frac{1}{\eta}\frac{D}{d^2}\frac{1}{\zeta}. \tag{6.11}$$

With this model we get for bilayer graphene with $\zeta = 100$, $\nu = \nu_{\mathrm{LS}}$, $d = 0.3$ nm and the typical graphene value $D \approx 0.02\ \mathrm{m}^2/\mathrm{s}$

$$\Gamma_{\mathrm{BLG}} \approx 10^{15}\ \mathrm{s}^{-1}. \tag{6.12}$$

For our system we have $\eta \sim 50$ while the other parameters stay the same and get therefore

$$\Gamma_{\mathrm{LS}} \approx 2 \times 10^{13}\ \mathrm{s}^{-1}. \tag{6.13}$$

This value gives the order of magnitude of the coupling rate between the localized states and the graphene channel. With this value we are in the limit of strong coupling of the system as depicted in Fig. 2 of the main text.